Available online at www.sciencedirect.com
ScienceDirect
Journal of Nuclear Materials 367–370 (2007) 166–172
journal of nuclear materials
www.elsevier.com/locate/jnucmat

Influence of particle dispersions on the high-temperature strength of ferritic alloys

D.T. Hoelzer [a,*], J. Bentley [a], M.A. Sokolov [a], M.K. Miller [a], G.R. Odette [b], M.J. Alinger [c]

[a] Oak Ridge National Laboratory, Metals and Ceramics Division, Oak Ridge, TN 37831-6151, USA
[b] University of California Santa Barbara, Santa Barbara, CA 93106-5070, USA
[c] University of California, Berkeley, CA 94720, USA

Abstract

Four ferritic alloys based on the composition Fe–14Cr–3W–0.4Ti (nominal wt%) were developed with a predominant dispersion of either oxide particles or nano-size Y-, Ti-, O-rich clusters, or nanoclusters (NC). Tensile specimens machined from the alloys were tested at room temperature and at temperatures ranging from ~360 °C to 800 °C in air using a strain rate of 10^{-3} s^{-1}. The results showed that the high-temperature strength of the NC strengthened alloys was significantly better than that of the oxide strengthened alloys. The room temperature yield strengths of the two alloys containing the NC were 1469 MPa and 1261 MPa while the yield strengths of the two oxide dispersion alloys were 819 MPa (Y–Ti-oxides) and 583 MPa (Ti-oxides). However, the ductility of the oxide strengthened alloys was better than that of the NC strengthened alloys.

1. Introduction

The dispersion of oxide particles in ferritic alloys by mechanical alloying (MA) is a well known process for improving their high-temperature strength and creep properties. In recent years, advances in understanding the MA process have resulted in creating a new type of material, namely, nano-structured ferritic alloys (NFA) that contain a high number density of Ti-, Y-, and O-rich nano-size clusters, or nanoclusters (NC). These NC were discovered in 1999 by three-dimensional atom probe (3-DAP) in a MA Fe–12Cr–3W–0.4Ti + $0.25Y_2O_3$ (nominal wt%) ferritic alloy, referred to as 12YWT, that was produced during the 1990s by Kobe Steel Ltd., in Japan [1,2]. Nanoclusters with similar size and composition characteristics to those studied in 12YWT have also been discovered by 3-DAP in the INCO MA957 alloy that was patented in 1978 [3,4]. The NC are a highly-defective non-equilibrium phase with the solute atoms occupying the lattice sites of the bcc Fe matrix. However, studies have shown that NC are thermally stable for long durations at temperatures up to ~800 °C and for short time at temperatures approaching 1300 °C [5,6]. They are primarily responsible for the marked improvement in high-temperature tensile and

* Corresponding author. Tel.: +1 865 574 5096.
E-mail address: hoelzerd@ornl.gov (D.T. Hoelzer).

0022-3115/$ - see front matter © 2007 Published by Elsevier B.V.
doi:10.1016/j.jnucmat.2007.03.151

thermal creep properties that has been observed for 12YWT and MA957 compared to conventional ferritic alloys and oxide-dispersion strengthened (ODS) ferritic alloys [7,8]. Thus, the combination of good thermal stability and high number density make NC dispersions very attractive for improving the high temperature strength of ferritic alloys.

In this study, four ferritic alloys based on Fe–14Cr–3W–0.4Ti were developed by MA with different particle dispersions. These alloys resulted from research covering ~5 years studying the effects of composition and processing conditions on the formation of particle dispersions and are not part of a systematic study. The primary purpose of this study was to produce different particle dispersions consisting of predominantly either oxide particles or NC and then compare their effects on the high-temperature tensile properties of the four MA ferritic alloys.

2. Experimental

2.1. Materials

Pre-alloyed powders with the nominal compositions intended to be close to Fe–14Cr–3W–0.4Ti (wt%) were produced by Special Metals, Inc. (SM) and Crucible Research (CR) using the argon gas atomization method. Four 200 g samples of pre-alloyed powders were prepared and given identifying codes of 14YWT-CR2, 14YWT-CR4, 14YWT-SM1, and 14YWT-SM4 (note: only the code following the hyphen will be mentioned in this article). One sample was ball milled with no Y_2O_3 addition (SM1) and three samples were ball milled with either 0.25 wt%Y_2O_3 (CR2) or 0.3 wt%Y_2O_3 (CR4 and SM4). The Y_2O_3 powder was supplied by Nanophase, Inc. and was reported to have a particle size ranging from 17 to 31 nm. The powders were ball milled using a Zoz Simolayer CM attritor mill in an Ar atmosphere for 40 h (CR4, SM1, and SM4) and 80 h (CR2) with a ball-to-powder mass ratio of 10:1. The CR2 alloy was developed during the initial phase of the research programs at ORNL when a milling time of 80 h was used. However, later it was determined that milling to 40 h produced similar grain sizes and lattice strains (from XRD analysis) as in the 80 h milling time and also lowered the contamination of the powders, which is inherent of ball milling. The milled powder was transferred to a 50 mm diameter mild steel can (a stainless steel can was used for CR2), degassed in a vacuum of $\sim 10^{-2}$ mbar at 400 °C, and sealed. The CR2 powder was extruded at 1175 °C while those of CR4, SM1, and SM4 were extruded at 850 °C. The chemical analysis of the major alloying elements indicated that base composition (in wt%) of the SM alloys was Fe–14.24%Cr–1.95%W–0.22%Ti and of the CR alloys was Fe–14.07%Cr–2.82%W–0.23%Ti.

2.2. Microstructural characterization

The microstructure and particle dispersions produced in the mechanically alloyed ferritic alloys was characterized using scanning electron microscopy (SEM), transmission electron microscopy (TEM), and energy-filtered TEM (EFTEM). Metallographic specimens for SEM analysis were prepared normal and parallel to the extrusion direction of the alloys and examined on a Philips XL30 Field Emission Gun (FEG) SEM operating at 5 kV. For TEM analysis, 3 mm diameter disk specimens were cut by wire electro-discharge machining (EDM) in directions normal and parallel to the extrusion direction of the alloys. The specimens were mechanically thinned to ~100 μm thickness and electro-polished in a Tenupol-3 using an electrolyte solution of 75% methanol and 25% nitric acid at ~−27 °C. The general microstructural characterization of extruded and annealed alloys was performed using a FEI Tecnai20 TEM at 200 kV equipped with EDAX energy-dispersive spectrometer (EDS). Imaging the NC proved to be unreliable using conventional bright- and dark-field (BF and DF) TEM. However, EFTEM using a LaB_6 Philips CM30 at 300 kV equipped with a Gatan imaging filter (GIF) was found to be more reliable in detecting NC by elemental mapping of Fe and Ti. The Fe M jump-ratio images showed the highest sensitivity to local changes in Fe composition and could reliably image NC with a spatial resolution approaching 1 nm [9]. Titanium L_{23} elemental mapping revealed the NC but were generally noisier than the Fe M jump-ratio images due to a lower sensitivity. Unfortunately, O and Y elemental mapping was often unsuccessful using EFTEM mainly because the unavoidable surface oxide that formed on the TEM specimens dominated the O signal and the Y M_{45} showed low sensitivity.

The nano-scale particle dispersion and solute distribution of the four alloys were characterized by atom probe tomography [10]. The atom probe specimens were prepared by standard electropolishing

methods. The 3-dimensional atom probe (3-DAP) characterizations were performed with a specimen temperature of 50–60 K, a pulse repetition rate of 1.5 kHz, and a pulse fraction of 20% of the standing voltage. For the local electrode atom probe (LEAP) analyses, a specimen temperature of 60 K, a pulse repetition rate of 200 kHz and a pulse fraction of 20% were used. The quantitative analysis of nano-size particles in the alloys was determined with the maximum separation method [10,11]. The results of the characterization of the CR4, SM1 and SM4 alloys in the as-extruded and 1000 °C annealed condition using the LEAP have been published [12]. The CR2 alloy was characterized using the 3-DAP.

2.3. Tensile test

Material of each as-extruded alloy was heat treated for 1 h at 1000 °C in a vacuum of $\sim 10^{-6}$ mbar and warm rolled to ~40% reduction-in-thickness at 600 °C. Flat sheet SS-J3 tensile specimens were EDMed from the rolled plate samples of each alloy with a nominal gage length of 5 mm and a gage thickness of 0.75 mm. The SS-J3 specimens were annealed for 1 h at 1000 °C before the tensile tests. The tensile tests were conducted in air at room temperature and at elevated temperatures ranging from ~364 °C to 800 °C using a strain rate of 10^{-3} s^{-1} on a MTS HYD-02 machine with a 1 kg load cell.

3. Results and discussion

3.1. Microstructural characterization

The microstructures of the four MA ferritic alloys were characterized by TEM and SEM after hot extrusion and 1000 °C anneal and were found to consist of very small grains and particle dispersions that depended on differences in composition and processing conditions. Fig. 1 shows representative bright-field (BF) TEM micrographs of the microstructures observed in the four alloys after annealing. The grains were slightly elongated parallel to the extrusion direction with a length-to-width aspect ratio of ~1–5. The SEM revealed at low magnifications the presence of stringers of sub-micron to micron size grains surrounded by nano-size grain regions in the alloys. However, the volume fraction of coarse grain stringers was very low in the SM1,

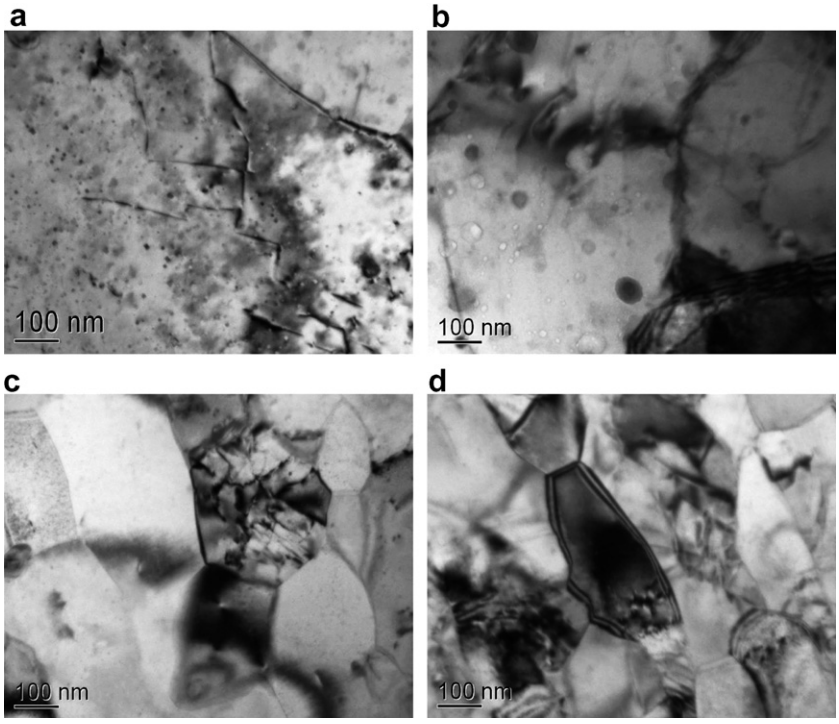

Fig. 1. Bright-field TEM micrographs showing the particle dispersions that were observed in the microstructures of the (a) CR2, (b) SM1, (c) CR4, and (d) SM4 alloys.

SM4 and CR4 alloys but was quite large (~38%) in the CR2 alloy. This larger fraction of coarse size grains in CR2 was mainly due to the higher extrusion temperature of 1175 °C compared to 850 °C that was used for SM1, SM4, and CR4. The lower extrusion temperature also resulted in smaller grain sizes. The qualitative analysis of grain size in the alloys showed the smallest grains (~0.5 μm diameter) in the CR4 and SM4 alloys. The grain size in the SM1 alloy, excluding the low fraction of coarse grains, was ~1 μm diameter. The grain size observed in the CR2 alloy varied from ~0.5 μm in regions containing small grains to ~2.0 μm in regions containing large grains.

The particle dispersions that were observed in the annealed alloys by TEM consisted of a low number density of sub-micron size carbide particles and distributions of sub-micron size oxides particles that varied in crystalline phase, size, and number density with alloy composition and processing conditions. The carbide particles were consistent with $M_{23}C_6$, where M = mixture of Cr, Fe, and W and were inhomogeneously distributed in the microstructure of the alloys. A relatively high number density of oxide particles was visible by diffraction contrast imaging in the CR2 (Fig. 1(a)) and SM1 (Fig. 1(b)) alloys. The SM1 alloy contained no Y_2O_3 additions resulting in a dispersion of TiO_2 particles with an average size in diameter ($\langle d \rangle$) of $\langle d \rangle = 8.7 \pm 4.5$ nm. The higher extrusion temperature used for consolidating the CR2 alloy resulted in the formation of several different oxide phases. The majority of oxide particles that formed within the grains were identified as the $Y_2Ti_2O_7$ phase with ($\langle d \rangle$) = 19.8 ± 7.6 nm. However, a lower number density of TiO_2 particles ($\langle d \rangle \cong$ 50–200 nm) and $Y_2Si_2O_7$ particles ($\langle d \rangle \cong$ 100–300 nm) were also observed both on grain boundaries and within grains. It should be noted that the particle size of the $Y_2Ti_2O_7$ phase in CR2 and TiO_2 phase in SM1 was determined from Fe M jump-ratio images that were obtained by EFTEM analysis (described below) while the larger size particles of the TiO_2 and $Y_2Si_2O_7$ phases in CR2 were determined by TEM analysis. The microstructure that was characteristic of the CR4 (Fig. 1(c)) and SM4 (Fig. 1(d)) alloys showed a low number density of both oxide and carbide phases. In general, the oxide particles that were observed in these two alloys contained Ti and O and were normally larger than ~10 nm in size.

The EFTEM analysis of the four alloys showed the presence of particles ~10 nm in all of the alloys. Fig. 2 shows Fe M jump-ratio images that reveal the nano-size particle (NP) dispersions present in the CR2 (Fig. 2(a)) and CR4 (Fig. 2(b)) alloys. The particles show dark contrast in the FeM jump-ratio image due to depletion of Fe. Although not shown, the depleted Fe regions associated with particles correlated with bright contrast in TiL_{23} jump-ratio images indicating the particles were enriched in Ti [9]. The results indicate that a high number density of relatively homogeneously distributed NP were present in the CR4 alloys. Similar results to these were also obtained from the EFTEM analysis of the SM1 and SM4 alloys, i.e. a low number of NP was observed in the SM1 alloys and a high number density of NP was observed in the SM4 alloy. The NP in the CR4 and SM4 alloys were usually ~5 nm in diameter and were observed in the grains and on grain boundaries. The very fine grain size

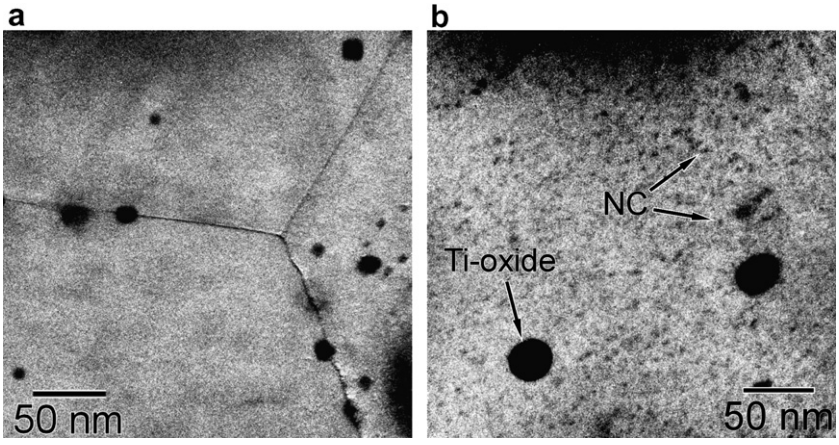

Fig. 2. EFTEM composition maps of the Fe M jump ratio showing the particle dispersions in the (a) CR2, and (b) CR4 alloys.

observed in these alloys may be attributed to the decoration of grain boundaries with the NP. In contrast, the NP in the CR2 and SM1 alloys had low number densities and were inhomogeneously distributed in grains and on grain boundaries. The NP in these alloys were most likely smaller oxide particles of those identified by TEM and XEDS.

The LEAP analysis of the CR4, SM4, and SM1 alloys revealed a high number density of Ti-, Y-, and O-enriched NC in the CR4 and SM4 alloys and a much lower number density of Ti-, O-enriched particles in the SM1 alloy [12]. The analysis of the CR2 alloy using the APT did not detect any particles including NC. It should be noted that the APT and LEAP data sets for the SM1 and CR2 alloys either did not contain any particles or contained one or two Ti-, O-enriched particles. Thus, the results from this technique were not appropriate for the quantitative analysis of the size and number density of the particles in these alloys. Fig. 3 shows the atom maps of Ti, Y, and O obtained by LEAP of the annealed SM4 alloy. The NC in CR4 were similar in size, number density and composition. The distribution of the NC was not uniform and some layering of NC was observed possibly due to an inhomogeneous distribution of solute atoms during milling or the presence of grain boundaries, which would affect the atomic diffusion and nucleation processes. The distribution of the Y in the NC is diffuse making it difficult to observe mainly because the LEAP data set contains a large number of Y atoms in a large field of view with many of the Y atoms distributed in the matrix. However, the maximum separate envelope method was used to determine the Y content of the NC. The LEAP analysis indicated that the 1000 °C annealing of CR4 and SM4 resulted in no statistical changes in size, number density or composition of the NC compared to the as-extruded condition. Following the annealing, the average size (Guinier radius, r_{nc}) of the NC was $r_{nc} = 0.9 \pm 0.2$ nm for SM4 and $r_{nc} = 1.0 \pm 0.2$ nm for CR4. The CR4 alloy contained a slightly higher number density ($\sim 7 \times 10^{23}$ m^{-3}) of NC compared to the SM4 alloy ($\sim 1 \times 10^{23}$ m^{-3}). The composition analysis indicated that the NC contained mostly Ti and O with a nearly 1:1 stoichiometric ratio and a smaller concentration of Y. The average composition of the NC in SM4 was Fe–43.9 ± 6.7%Ti–6.9 ± 5.8%Y–44.7 ± 4.0%O–1.1 ± 1. 1%Cr and in CR4 was Fe–37.6 ± 8.6%Ti–12.3 ± 8.8%Y–44.4 ± 4.6%O–1.2 ± 1. 2%Cr. Thus, the results indicated the NC detected in CR4 and SM4 were similar to the those studied in the 12YWT and MA957 alloys [7,8].

3.2. Tensile tests

One of the primary objectives of this study was to compare the effect of different particle dispersions in two pairs of alloys (SM1/SM4 and CR2/CR4) on the high-temperature tensile properties. The primary difference in the preparation of the CR2 and CR4 alloys was the extrusion temperature: CR2 was extruded at 1175 °C and CR4 at 850 °C. The higher extrusion temperature resulted in a predominant oxide dispersion of $Y_2Ti_2O_7$ while the lower consolidation temperature resulted in the formation of the Ti-, Y-, and O-rich NC. The SM1 and SM4 alloys were extruded at 850 °C, however, SM1 was ball milled with the same conditions but without Y_2O_3. Thus, a NC dispersion formed in SM4 and but a TiO_2 dispersion formed in SM1.

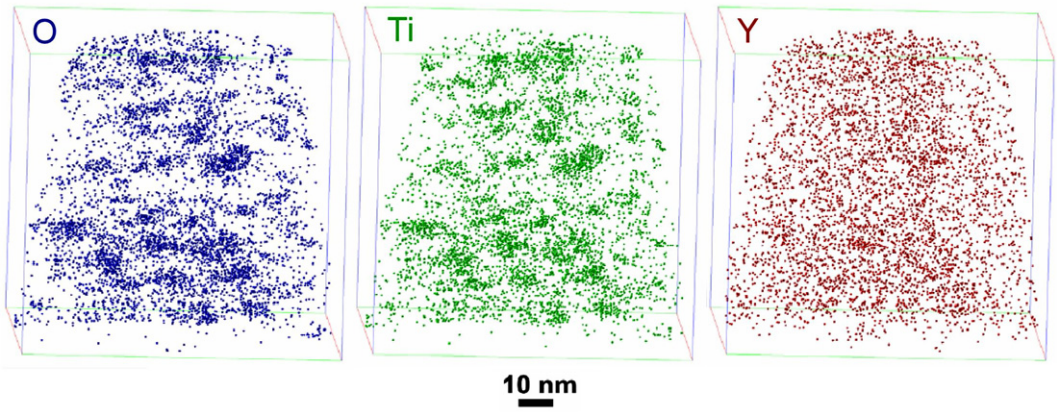

Fig. 3. Composition maps of Ti, Y, and O showing the high number density of nanoclusters that were detected by LEAP in the SM4 alloy.

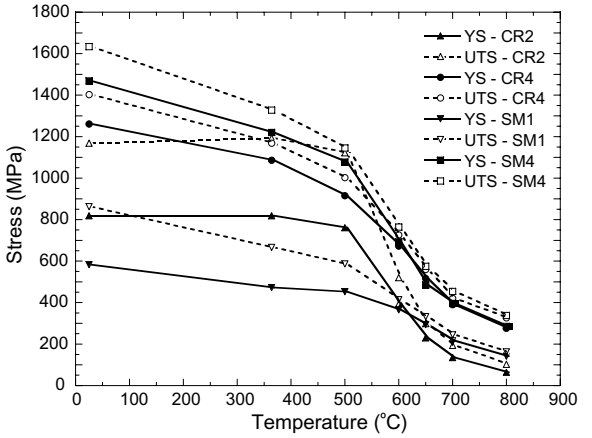

Fig. 4. Plot comparing the yield and ultimate tensile strengths measured as a function of temperature up to 800 °C for the CR2, CR4, SM1, and SM4 alloys.

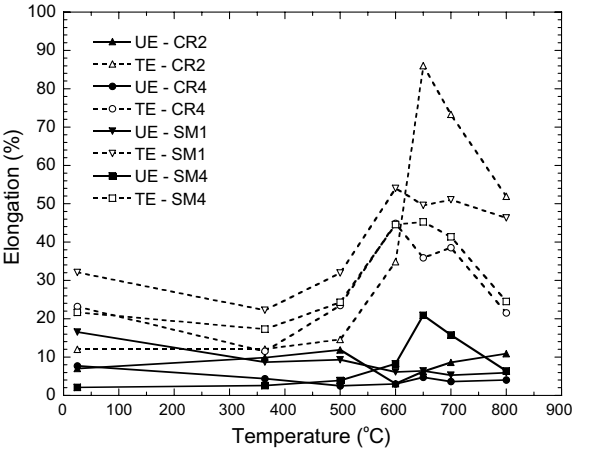

Fig. 5. Plot comparing the uniform and total elongation measured as a function of temperature up to 800 °C for the CR2, CR4, SM1, and SM4 alloys.

Fig. 4 shows the effect that the different dispersions had on the strengthening behavior of the four alloys from room temperature to 800 °C. The results show that the high number density of NC in the SM4 and CR4 alloys provided significant strengthening over the oxide dispersions in the SM1 and CR2 alloys for the entire temperature range. A room temperature yield strength (σ_{ys}) of 1469 MPa was measured for the SM4 alloy and this was 886 MPa higher than that of the SM1 alloy ($\sigma_{ys} = 583$ MPa). Similarly, the σ_{ys} for CR4 alloy was 1261 MPa and was 819 MPa for the CR2 alloy at room temperature. A higher σ_{ys} was measured in the SM4 and CR4 compared to the SM1 and CR2 at all test temperatures up to 800 °C. The same trend was essentially observed with the ultimate tensile strength (σ_{uts}). There were no significant differences in strengthening above ~500 °C between the NC dispersions that were present in the SM4 and CR4 alloys. However, the $Y_2Ti_2O_7$ oxide particles in CR2 provided higher strengthening below ~600 °C, but above this temperature the TiO_2 oxide particles in SM1 provided higher strengthening.

On the other hand, the oxide dispersions in SM1 and CR2 resulted in better ductility compared to the NC dispersions in SM4 and CR4 as shown in Fig. 5. The uniform elongation (UE) was typically ~6% for SM4 and CR4 over most of the temperature range. The UE for CR4 at room temperature was 7.7%, which was surprisingly comparable to that of CR2. In addition, the UE of SM4 was larger than that of SM1 above 600 °C: the UE in this alloy was 8.3% at 600 °C and increased to a peak of ~21% at 650 °C. The total elongation (TE) of the NC strengthened alloys was not significantly different from that of the oxide strengthened alloys. All of the alloys showed an increase in TE starting at ~500 °C, reaching a peak near 600–650 °C. The very fine grain size in SM4 and CR4 may be partly responsible for the relatively high TE. Furthermore, the increase in TE above 500 °C occurs concomitantly with the sudden decrease in strength observed in the four alloys in Fig. 4. The reason for this is not known but will be the focus of future research.

4. Summary

Two pairs of ferritic alloys based on Fe–14Cr–3W–0.4Ti were prepared using different MA conditions to study the effect of different particle dispersions on their high temperature tensile properties. The pair of alloys that were ball milled with 0.25–0.3%Y_2O_3 and extruded at different temperatures was found to contain high number density of Ti-, Y-, and O-rich NC after extrusion at 850 °C (CR4) and a lower number density of predominantly $Y_2Ti_2O_7$ oxide particles after extrusion at 1175 °C (CR2). Another pair of alloys was extruded at 850 °C, however, the alloy ball milled with 0.3%Y_2O_3 (SM4) also contained a high number density of NC but the alloy ball milled without Y_2O_3 (SM1) contained a lower number density of TiO_2 particles. The tensile tests revealed significant increases in yield and ultimate tensile strengths from room temperature to 800 °C in the NC strengthened

SM4 and CR4 alloys compared to their counterpart oxide dispersion strengthened SM1 and CR2 alloys, respectively. On the other hand, the oxide dispersion strengthened alloys showed better ductility properties compared to the NC strengthened alloys over the test temperature range.

Acknowledgements

Research at Oak Ridge National Laboratory (ORNL) and the University of California Santa Barbara (UCSB) was primarily sponsored by the US Department of Energy Office of Nuclear Energy, Science and Technology (I-NERI 2001-007-F), and the ORNL Laboratory Directed Research and Development Program. Research at the ORNL SHaRE Facility was supported in part by the Division of Scientific User Facilities, Office of Basic Energy Sciences, US Department of Energy. ORNL is managed by UT-Battelle, LLC for the US Department of Energy under Contract No. DE-AC05-00OR22725.

References

[1] D.J. Larson, P.J. Maziasz, I.S. Kim, K. Miyahara, Scripta Mater. 44 (2001) 359.
[2] I.S. Kim, B.-Y. Choi, C.-Y. Kang, T. Okuda, P.J. Maziasz, K. Miyahara, ISIJ Int. 43 (10) (2003) 1640.
[3] M.K. Miller, E.A. Kenik, K.F. Russell, L. Heatherly, D.T. Hoelzer, P.J. Maziasz, Mater. Sci. Eng. A A353 (2003) 140.
[4] J.J. Fisher, 'Dispersion Strengthened Ferritic Alloy for use in Liquid Metal Fast Breeder Reactors,' US Patent 4,075,010, issued February 21, 1978.
[5] M.K. Miller, D.T. Hoelzer, E.A. Kenik, K.F. Russell, J. Nucl. Mater. 329–333 (2004) 338.
[6] M.K. Miller, D.T. Hoelzer, E.A. Kenik, K.F. Russell, Intermetallics 13 (2005) 387.
[7] R.L. Klueh, P.J. Maziasz, I.S. Kim, L. Heatherly, D.T. Hoelzer, N. Hashimoto, E.A. Kenik, K. Miyahara, J. Nucl. Mater. 307–311 (2002) 773.
[8] R.L. Klueh, J.P. Shingledecker, R.W. Swindeman, D.T. Hoelzer, J. Nucl. Mater. 341 (2005) 103.
[9] J. Bentley, D.T. Hoelzer, D.W. Coffey, K.A. Yarborough, Microsc. Microanal. 10 (suppl. 2) (2004) 662CD.
[10] M.K. Miller, Atom Probe Tomography, Kluwer Academic/Plenum, New York, 2000.
[11] M.K. Miller, E.A. Kenik, Microsc. Microanal. 8 (Suppl. 2) (2002) 1126CD.
[12] M.K. Miller, K.F. Russell, D.T. Hoelzer, J. Nucl. Mater. 351 (2006) 261.